NiCu anchored on specific TiO_2 face tuning electronic density dominating fatty acid selective hydrogenation into alkane or alcohol

Feng Long[1], Xincheng Cao[1], Xia Jiang[1], Peng Liu[1], JianChun Jiang[1,2], Xiaolei Zhang[3], Junming Xu*[1,2].

1. Institute of Chemical Industry of Forest Products, Chinese Academy of Forestry; Key Lab. of Biomass Energy and Material, Jiangsu Province; Key Lab. of Chemical Engineering of Forest Products, National Forestry and Grassland Administration; National Engineering Lab. for Biomass Chemical Utilization, Nanjing 210042, China

2. Co-Innovation Center of Efficient Processing and Utilization of Forest Resources, Nanjing Forestry University, Nanjing 210037, China

3. Department of Chemical and Process Engineering, University of Strathclyde, Glasgow, G11XJ, UKs

Corresponding author

Junming Xu- Institute of Chemical Industry of Forest Products, Chinese Academy of Forestry; Key Lab. of Biomass Energy and Material, Jiangsu Province; Key Lab. of Chemical Engineering of Forest Products, National Forestry and Grassland Administration; National Engineering Lab. for Biomass Chemical Utilization, Nanjing 210042, China. Co-Innovation Center of Efficient Processing and Utilization of Forest Resources, Nanjing Forestry University, Nanjing 210037, China.

Email: xujunming@icifp.cn

Abstract: Catalyst design is critical for renewable selective hydrogenation of fatty acids into alkane or alcohol, especially for active metal and support. We demonstrate NiCu anchored on TiO_2 (P25) surface, prepared by the impregnation method, performed superior temperature-sensitive catalytic activities with a higher fatty alcohol yield of 78.2% (205°C, 4 MPa H_2 and 12 h), and alkane yield of 85.0% (245°C, 3 MPa H_2 and 6h), respectively. X-ray photoelectron spectroscopy (XPS) and density functional theory (DFT) suggest that Ni or NiCu anchored on oxygen vacancies rutile can achieve reversal charge transfer between metal and TiO_2 support. Especially the normal NiCu cluster loading on rutile surface can improve the dispersion of NiCu cluster and oxygen vacancy concentration. Thus, more NiCu clusters anchored on oxygen deficiency can obtain negative charges in favor of alcohol production. In contrast, the other active

NiCu clusters will preferentially cleavage the C−C bond to produce alkane under a higher reaction temperature. Our work provides a new strategy for designing highly effective hydrogenation catalysts.

Keywords: hydrogenation, diesel-like alkanes, fatty alcohol, electron density, DFT calculation.

Synopsis: Bio-derived fatty acid conversion into diesel-like alkane or chemical fatty alcohol can improve it sustainability and value.

INTRODUCTION

In the context of international carbon neutrality and carbon peaking, the limited availability of fossil raw materials for fuel and chemical production, supply dependence, and related environmental issues has facilitated the use of biomass-based resources[1, 2]. As we all know, biomass materials such as animal fats, vegetable oils and waste oils, mainly composed of triglycerides and fatty acids, with a molecular structure similar to petroleum oil, can be converted to renewable diesel-like alkanes and high-valuable fatty alcohols[3]. Moreover, the transformed alkane or alcohol utilized can significantly meet the requirement of carbon neutrality rules.

It is reported that the hydrogenation process was a primary conversion method for the bio-derived fatty acids transforming into an alkane. In earlier research, traditional NiMoS and CoMoS catalysts were used in the catalytic hydrodeoxygenation process. Yet, sulfur pollution or sulfur leaching limits their utilization[4]. Then, metal-based phosphide/nitride/carbide catalysts also used in the hydrogenation conversion, such as NiP, Mo_2C/N and NiC, which can effectively convert the fatty acid into alkanes[5]. However, the catalyst prepared method always needed a harsh preparation process, making it challenging to achieve industrialization. After that, the noble metals catalysts with great activity and durability also have been reported in this field. But the high cost of the noble metal undoubtedly limits its application[6]. Hence, a cost-efferent and sulfur-

free catalyst has attracted extensive attention, such as transition metals and alloys. Especially Ni-based catalysts, due to the low-cost Ni metal, show remarkable hydrogen dissociation activity, which can perform excellent reaction activity in fatty acid conversion[7].

It is commonly known that the hydrogenation conversion of fatty acids into alkane is mainly carried out through hydrodeoxygenation, decarbonylation, and decarboxylation three processes, which are removed the O atom as the form of H_2O, CO and CO_2, respectively [8]. Among these, it was found that fatty alcohols can be detected as an essential intermediate during the hydrodeoxygenation processes. Thus, the production of high value-added fatty alcohols by stopping the hydrogenation reaction in the alcohol stage has been attracted growing attention. From the 1930S to the present, the Adkins-type $CuO/CuCr_2O_4$ catalyst is still applicable to produce fatty alcohols on an industrial scale, with alcohol yield higher than 90% under the 200-300℃, 20-30 MPa conditions[9, 10, 11]. However, the environmentally unfriendly Cr-based catalyst and harsh reaction conditions actuate the research towards a new type of catalyst. Various noble-metal catalysts, such as Ru, Rh, Re, Pd and Pt [12, 13, 14, 15], have been applied to achieve high yield fatty alcohol production under a mild reaction condition, 130-150℃, 2 MPa H_2 pressure. For example, Hardacre et al. [16] have found that, under 130°C and 2 MPa H_2, the acid conversion and selectively to alcohol reach 82% and 93% over the Pt/TiO_2 catalyst, respectively. Additionally, a Pd/Re/C catalyst was realized to carboxylic acids for the selective preparation of either alcohol (130℃, 2 MPa) or the alkane (160℃, 3 MPa)[17]. Although the noble-metal catalysts show outstanding activity for fatty alcohols production, a cost-effective and environment-friendly catalyst to replace the noble metal should be investigated without delay.

At present, Cu-based catalysts are still a research hotspot due to the high selectivity to fatty alcohols[18]. Generally, another metal, such as Zn, Fe and In was added to modify the catalyst activity[10, 12, 18]. It is reported that the ally or intermetallic compound can provide react sites for active H_2, adsorb ester group or prevent the hydrogenation reaction from staying in the stage of the alcohol. For example, Kapil Kandel et al[10].

reported that fatty acids could be converted into alcohols over $CuFeO_x/SiO_2$ catalyst under moderate conditions (180°C,3 MPa H_2). It was proposed that copper could be H_2 activation site and iron oxide could bind and activate the carboxylic acid, in which the acid could be converted into alcohol with a yield reaching 95%. In addition, In was used to modify Cu to form CuIn alloy, which can suppress the dehydration reaction for enhancing the selectivity of alcohols[19]. On the other hand, Ni-based catalyst has also been investigated due to its higher hydrogenation activity and resistance to sintering. But the Ni metal is more active in deoxygenation and C-C bond cracking, which can produce undesirable alkane products. Therefore, the over hydrogenation reaction can be inhibited by modifying another metal (In or Fe) or appropriate metal oxide[18, 20]. Such as the NiFe alloy oxide catalyst can provide the steric hindrance of lattice oxygen to inhibit the further conversion of alcohol, which can reach 100% conversion and 90% selectivity for lauric acid converted to lauryl alcohol[7]. Inspire by these foundings, we think the Ni and Cu combination could be a good candidate for the alcohol production.

Besides the active metal site, the support also participates in the reaction as an important role. The supports include active carbon, Al_2O_3, ZrO_2, SiO_2 and TiO_2[10-12, 15, 21], and their major factor, including Lewis sites, oxygen vacancy and crystal structure can effect the hydrogenation conversion. Besides, the synergistic effect between the support and metal active site can promote the desired reaction for alcohol or C_{n-1}/C_n alkane production [14, 18, 22]. As we all know, the catalyst activity is highly influenced by their electronic states, including the electron gain and loss between metal site and support and the electron state of the metal site. For example, Jun Ni et al[1]. prepare different crystal phases ZrO_2 with rich oxygen vacancy to carrier the Ni metal for fatty acid conversion. They found that the higher excess electron density Ni metal can promote fatty alcohol production, and the Ni metals with approximate excess electron density are more likelihood to produce alkanes. Thus, a research strategy that can achieve selective production of fatty alcohols and alkanes from fatty acids by studying the structural states of support and the electronic status of active metals.

This paper demonstrates that introducing Cu in the NiCu can increase the metal

dispersion and oxygen vacancy concentration. The normal NiCu cluster anchored on oxygen vacancies can change the electron density. Especially, rutile as the support can induce a unique effect, reversed charge transfer between metal and rutile support. Thus, a more negative charge exhibited in the NiCu/TiO_2 system promotes fatty acids hydrogenation to produce the fatty alcohol. In contrast, it cleaves the C-C bond to produce alkane under a higher temperature condition. The electronic transfer is also confirmed by XPS and DFT calculations. Our work provides an insight into the temperature-sensitive catalyst design, which effect by metal clusters and the support, for selective hydrogenation of fatty acid into alcohol or alkane.

EXPERIMENTAL SECTION

Materials

$Ni(NO_3)_2 \cdot 6H_2O$ and $Cu(NO_3)_2 \cdot 6H_2O$ are obtained from Macklin (Shanghai, China), with the purity of 98.0% and 98.5%, respectively. TiO_2(P25) with the anatase: rutile=8:2 and was purchased from Degussa. SBA-15 with a pore size between 6-11nm and a specific surface area between 550-600 m^2/g was purchased from XFNAO,INL(Nanjing, China). Nano ZrO_2 (purity, 99.99%) and SiO_2 (specific surface area of 200 m^2/g) were purchased from Aladdin (Shanghai, China), with pore size ≤100 nm. HZSM-5 with a specific surface area of 365 m^2/g was purchased from Nankai university Catalyst., Co., ltd. Nano anatase (purity, 99.8% and pore size= 25 nm), Nano rutile (purity, 99.8% and pore size= 25 nm) and Nano Al_2O_3 (purity, 99.99% and pore size=10 nm) were purchased from Macklin (Shanghai, China). Solvent cyclohexane (AR, 99.5%) was also obtained from Macklin (Shanghai, China). All the materials and chemicals were used with no further purification.

Catalyst preparation

In this work, a series of catalysts were prepared by three different methods, including impregnation (IM), coprecipitation (CP) and hydrothermal (HT) methods. The specific preparation procedures are shown in Scheme 1 and supporting information.

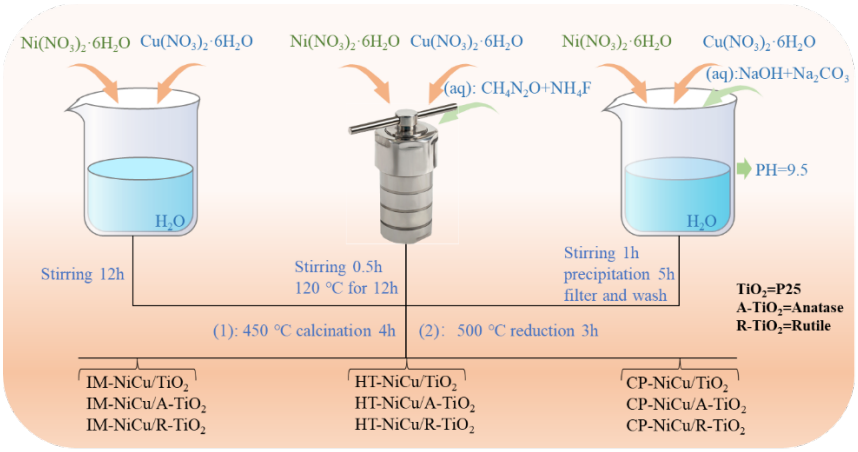

Scheme 1. The procedure of preparing various hydrogenation catalysts by three different methods.

Characterizations

X-ray diffraction (XRD) patterns were collected on a D8 FOCUS (Bruker Company, Germany) X-ray diffractometer was recorded from 2θ=10-80° and the instrument using the Cu-Kα (λ=0.15418 nm) radiation as the X-ray source at 40kV and 100mA. X-ray photoelectron spectra (XPS) were acquired on the ESCALAB 250 X-ray instrument, the XPS instrument using an Al-Kα source (hν=1486.6 eV) as the X-ray source. During deconvolution, the XPS data were corrected with C1s (284.48 eV), and the Gaussian type was applied. Transmission electron microscopy (TEM) and mapping images of all $NiCu_{1:1}$-TiO_2 were performed on FEI-TF20 electron microscopy with an operating voltage of 200kV. Electron paramagnetic resonance (EPR) spectra were performed on a Bruker EMXPlus EPR spectrometer recorded at 77 K using a 9.65 GHz operating frequency. Temperature-programmed reduction (H_2-TPR) was performed on an AUTO CHEM 2920 apparatus. And the detailed operating procedures: the catalyst sample was added to a quartz reactor and reduced in a mixture H_2-Ar gas with the flow of 50 mL/min with a temperature rate of 10℃/min until 800℃. N_2 adsorption-desorption isotherms of the catalysts were recorded on Micrometric ASAP 2020 instrument. Specific surface area and pore volume/average pore diameter were calculated by Brunauer-Emmett-Teller (BET) method and Barrett-Joyner-Halenda (BJH) method, respectively. NH_3 temperature-programmed desorption (NH_3-TPD) and CO-pulse chemisorption were measured on the AUTO CHEM 2920 instrument, and

their detail detailed operating procedures can be found in Supporting Information. The actual loading of all Ni or Cu was determined by inductively coupled plasma Optical Emission and Mass Spectrometer (ICP-MS) on Agilent 720ES (the results are listed in Table 1and Table S1).

Table.1 Properties of Ni, Cu and NiCu catalysts.

Catalyst	Metal content (wt%) [a]		Crystallite size (nm)	S_{BET} (m^2/g)[c]	V_P (cm^2/g)[c]	d_P (nm)[c]	CO uptake (μmol/g)[d]	Ni dispersion (%)[d]
	Ni	Cu	TEM[b]					
IM-Ni/TiO_2	9.18	-	14.3	52.3	0.13	205.2	49.9	2.93
IM-Cu/TiO_2	-	7.45	18.1	58.2	0.16	217.5	2.94	-
IM-NiCu/TiO_2	7.76	5.84	13.7	45.9	0.10	226.8	54.7	1.61

a: Measured by ICP-MS.

b: Obtained from TME images.

c: Obtained by BET data.

d: Measured by CO-pulse chemisorption

Hydrogenation reaction and product analysis

The tests of Ni and NiCu catalysts for selective hydrogenation of fatty acid were carried out in a 50 mL autoclave reactor. Typically, reduced catalyst (0.03 g), fatty acid (0.1 g) and 10 mL cyclohexane as solvent were added into the autoclave reactor. The autoclave reactor was purged H_2 five times to remove the air and then pressurized 3-4.5 MPa H_2 before the reaction. And then, the autoclave was heated from ambient temperature to 205-260℃ with a desired heating rate. After the reaction, cool down the reactor to room temperature and collect the liquid product. And undecane as the internal standard for quantitative calculation. Finally, the liquid product was quantitative using gas chromatography (GC, Agilent 7890A/5975C) and qualitative using gas chromatography-mass spectrometry (GC-MS, Agilent 6890/5973N). The GC and GC-MS test program is as follows: the vaporization chamber temperature was 280℃, the chromatographic column temperature was 150℃, and the detector temperature was 280℃. The oven temperature was firstly held at 150℃ for 2 min and then increased to 280℃ at a heating rate of 10℃/min, and then kept for 10 min at 280℃. All catalytic conversion experiments were repeated more than two times, and the data error was

within an acceptable range of less than 5%.

The conversion rate of fatty acid, selectively and yield of products were calculated as follows formula:

$$\text{Conversion } (\%) = \left(1 - \frac{m(feeddstock\ after\ reaction)}{m(feeddstock\ before\ reaction)}\right) \times \% \quad [1]$$

$$Selectively(\%) = \frac{m(product)}{m\ (total\ products)} \times \% \quad [2]$$

$$Yield\ (\%) = \frac{m(product)}{m\ (feedstock\ before\ reaction)} \times \% \quad [3]$$

DFT calculations

The density functional theory (DFT) was carried out by the Vienna Ab Initio Simulation Package (VASP)[23]. The general gradient approximation Perdew-Burke-Ernzerho (GGA-PBE) functional described the exchange and correlation energy[24]. Valence electrons were calculated on the plane-wave basis with a cutoff energy = 450 eV with a single Gamma-point only for Brillouin zone. And during the structure calculation, the convergence criteria for self-consistent calculation =10^{-4} eV, and the convergence threshold for forces <0.05 eV. GGA+U method was used for all calculations, the coulomb correlation interaction of Ti (Ueff=4.0 eV) and Ni (Ueff=3.8 eV) was used for 3d orbit for accurate accuracy calculation[25]. The adsorption energy (E_{ad}) of the Ni and NiCu cluster on TiO_2 surface was calculated as follows:

$$E_{ad} = E\ (Ni/TiO_2) - E(Ni) - E(TiO_2) \quad [4]$$

$$E_{ad} = E\ (NiCu/TiO_2) - E(NiCu) - E(TiO_2) \quad [5]$$

Both the rutile: a P(3×1) TiO_2 (110), and anatase: a P(1×3) TiO_2 (101) slabs are with 3 O-Ti-O tri-layer were built, 15 Å of vacuum and 3×3×1 k-point mesh were used, the bottom layer was fixed and the rest were allowed to relax.

Results & Discussion

Catalyst characterizations

XRD patterns of the TiO_2 support Ni, Cu and NiCu catalysts are shown in Figure 1, the intensive diffraction peaks at 2θ = 28.25, 37.80, 48.05, 53.89, 55.06 and 62.69° are the crystalline phases of anatase (JCPDS 21-1272), and the 2θ =27.45, 36.09, 41.23, 54.23 and 69.00° are representing the crystalline phases of rutile (JCPDS 21-1276),

which are observed from the calcined and reduced catalysts. As we can see from Figure 1a, which were the XRD patterns of the calcined catalysts, the diffraction peaks of CuO (2θ = 35.50, 38.73°, JCPDS 45-0973) and NiO (2θ = 37.25, 43.28, 62.88° JCPDS 47-1049) were weakly on the monometallic Ni of Cu catalyst, indicating good dispersion of the small NiO and CuO clusters on the TiO_2 surface. And in contrast, the NiCu catalyst exhibited obvious peaks of the crystal phase of CuO and NiO, suggesting that the interaction between the NiO and CuO exists. Additionally, the crystalline phases of TiO_2 were weakened, indicating Ni-O-Cu was formed and the NiCu is highly dispersion on the surface.

Interestingly, compared to the XRD patterns of the three reduced catalysts in Figure 1b, the monometallic Cu/TiO_2 shows no Cu^0 (JCPDS 04-0836) XRD peaks, confirming the Cu highly dispersion on the surface. Yet, as for monometallic Ni/TiO_2 catalyst, it shows obvious peaks at 2θ = 44.51, 51.85° (JCPDS 04-0850), which belong to the (111) and (200) reflections of the Ni metal, respectively. For the $NiCu/TiO_2$ reduced catalyst, it is noted that the XRD peak at the 2θ = 44.50° is sharper and more intense compared with the monometallic catalysts. Besides this, the typical anatase and rutile crystal phase peaks of the $NiCu_{1:1}/TiO_2$ catalyst are weakened, indicating that the Cu metals can promote the dispersion of Ni metals. What's more, the metal dispersion also can be effect by the Ni/Cu ratio. As Figure S1 shows, the Ni/Cu ratio greatly influences the crystal phase peaks of the TiO_2, the catalyst whose ratio is nearly Ni/Cu =1:1 with a higher dispersion NiCu cluster.

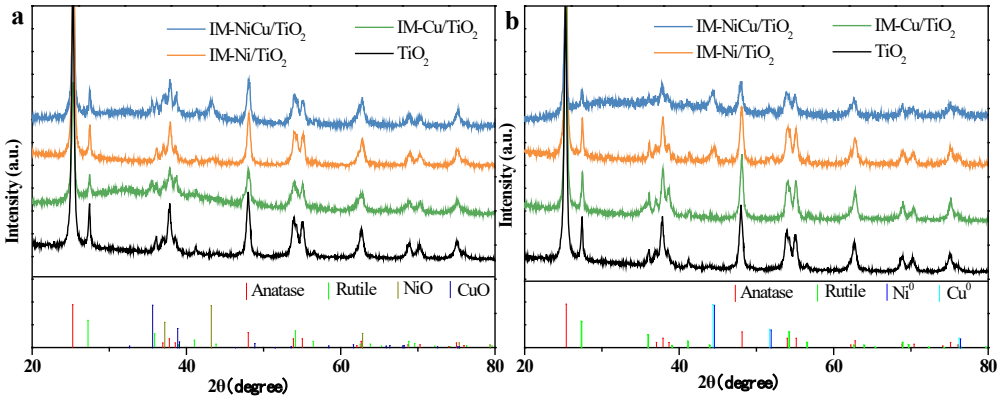

Figure 1. XRD patterns of the calcined catalysts (a) and reduced catalysts (b).

XPS was used to characterize the Ni, Cu, O and Ti oxidation state of the Ni, Cu and NiCu catalysts, and the result is shown in Figure 2 a-d. As we can see from Figure 2a, the Ni main peaks including $Ni^0 2p_{3/2}$, $Ni^{2+} 2p_{3/2}$ and $Ni^{0/2+} 2p_{1/2}$, and the main corresponding Ni peaks of Ni/TiO_2 are located as 852.2, 855.7 and 873.5 eV, respectively[26]. And a large peak area of NiO observed in the Ni $2p_{3/2}$ spectra is higher than the Ni^0 $2p_{3/2}$ spectra, which is attributed to the catalyst could be oxidation before their test in the XPS instrument. And although the binding energy (BE) of the Ni^0 $2p_{3/2}$ peak has a slight shift, the shoulder width of the Ni characteristic peaks has a significant change compared to the Ni and NiCu catalyst, which is due to the interaction between the Cu and Ni metal. In addition, the shift in BEs when comparing the Cu characteristic peaks between the Ni/TiO_2 and $NiCu/TiO_2$ catalysts, combining Ni and Cu into the system shifted the Cu^0 $2p_{3/2}$ maxima from 932.4 to 932.8 eV and the Cu^{2+} $2p_{3/2}$ peaks shifted from 933.6 to 934.3 eV, also demonstrating an interaction between the Ni and Cu metal.

XPS analysis was further performed to investigate the chemical states of the O and Ti in catalysts to evidence the existence of the oxygen vacancies (O_vs), shown in Figures 2 c and d. Figure 2 c shows the O1s spectra of the catalysts, which are deconvoluted into three signal peaks attributing the Ti^{4+}-O (lattice oxygen), Ti^{3+}-OH/·OH (hydroxyl group) and H_2O_{ads}/ Ti^{3+}-O (O_vs or chemisorbed water), at the BEs approximately of 529.8, 530.5 and 532.0 eV[27, 28]. It is noted that a higher proportion of H_2O_{ads}/ Ti^{3+}-O (29.6%) are found on the surface of the NiCu catalyst compared to the Ni/TiO_2 (20.6%) and Cu/TiO_2 (23.0%), detailed data are shown in Table S2. And Ti^{3+}-OH/·OH is similar to H_2O_{ads} with a proportion of 21.8%, which is higher than that Ni/TiO_2 (18.5%) and Cu/TiO_2 (19.4%). As we know, the H_2O is more likely to adsorb onto the O_vs sites and then convert into ·OH[29]. Therefore, the high proportion of H_2O_{ads}/ Ti^{3+}-O and Ti^{3+}-OH/·OH indicates that the highly concentrated O_vs exist on the $NiCu/TiO_2$ catalyst surface[28]. And the Ti 2p spectrum exhibits four contributions Ti^{3+} $P_{3/2}$, Ti^{4+} $P_{3/2}$, Ti^{3+} $P_{1/2}$ and Ti^{4+} $P_{1/2}$, resulting from the spin-orbit-splitting, which is located at approximately 458.4, 458.8, 464.0 and 464.6 eV, respectively (Figure 2d). The Ti 2P peaks of Ni/TiO_2

and Cu/TiO_2 are lower than the peaks of $NiCu/TiO_2$, indicating more pronounced charge transfers from TiO_2 slab to NiCu cluster in $NiCu/TiO_2$ catalyst. The following Bader calculation was also performed to probe the surface charge of the cluster and slab.

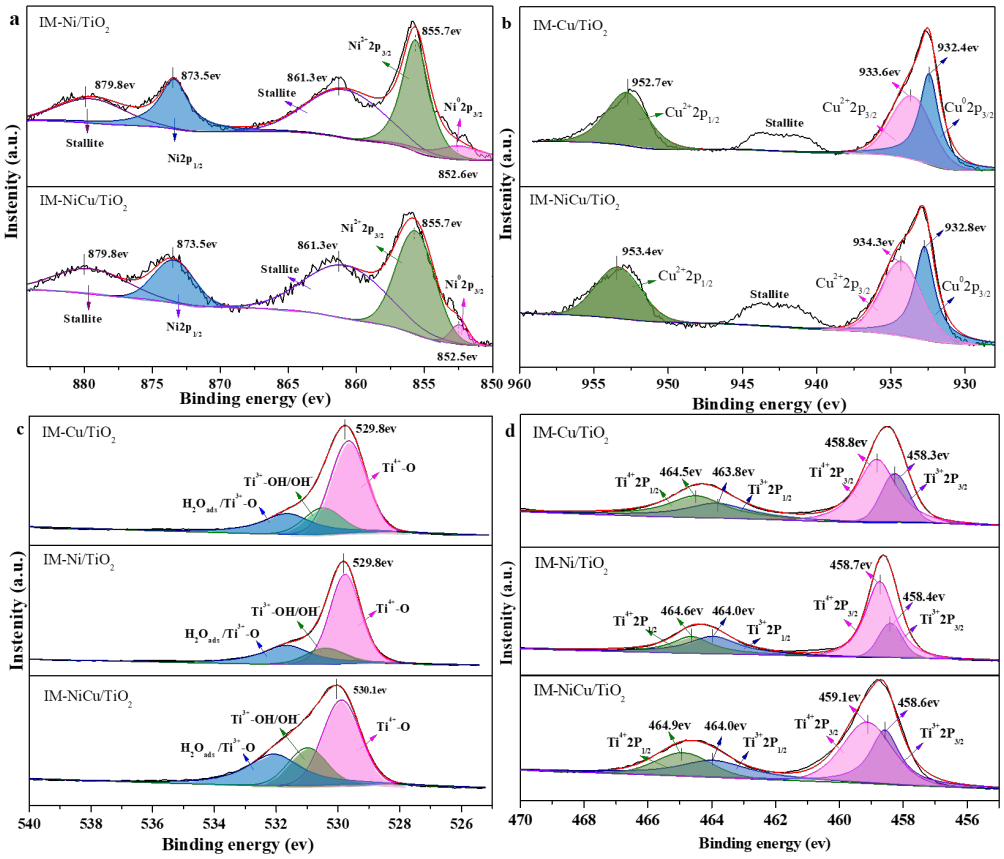

Figure 2. XPS spectra of Ni 2p (a), Cu 2p(b), O 1s (c) and Ti 2p (d) of reduce catalysts.

TEM and mapping were carried out to investigate the distributions and the particle sizes of the Ni, Cu and NiCu clusters on the TiO_2 surface, the results are shown in Figure 3. Many Ni and Cu particles were observed for the Ni/TiO_2 (Figure 3 A1) and Cu/TiO_2 (Figure3 B1), with an average size of ~14.3 nm and ~18.1 nm, respectively. The TEM results demonstrate that monometallic Ni or Cu and NiCu cluster were successfully dispersed on the TiO_2 surface. In contrast, weak adsorption energy of the monometallic Ni or Cu on the slab TiO_2 makes them easy to agglomerate to form large particles. Additionally, the $NiCu/TiO_2$ catalyst (Figure 3 C1) exhibited a smaller NiCu particles size of 13.7 nm, indicating the internal interaction of the Ni and Cu metal promotes the high dispersion and smaller partial size of the NiCu cluster, which is

consistent with XRD results. In addition, the CO chemisorption was carried out to measure the surface Ni metal density, and the results are listed in Table 1. As detailed in Table 1, the Ni/TiO_2 with a 2.93% Ni metal dispersion and the $NiCu/TiO_2$ catalyst showed a lower Ni metal dispersion of 1.61%, in line with the Ni metal content. But, the $NiCu/TiO_2$ catalyst performance a higher CO uptake value than the Ni/TiO_2 catalyst, which also indicates that Ni metal could be active by the Cu metal for a strong adsorption behavior. And following DFT calculation prove that NiCu cluster has higher adsorption energy on the TiO_2 surface, which also explanting the high dispersion and smaller partial size phenomenon.

And yet, the TEM was also used to verify NiCu cluster formation. As shown in Figure 3 A2, B2 and C2, a lattice spacing of 0.203 nm were detected, which belongs to the typical Ni (111). And the TEM image (Figure 1 C2) shows the $NiCu/TiO_2$ catalyst presents the face-centered cubic (FCC) lattice with the interlayer spacing of 0.206 nm, which match well with the NiCu (111) typical lattice, indicating the NiCu cluster state truly exist in the $NiCu/TiO_2$ catalyst[21, 30]. In addition, element mapping under the TEM mode aims to characterize the element distribution in the catalyst. The elemental mapping images (Figure 3, third row) showed that Ni and Cu species coexist in the $NiCu/TiO_2$ catalyst. The Ni and Cu are seen to agglomerate to form some small clusters, indicating the strong interaction between the Ni and Cu metal.

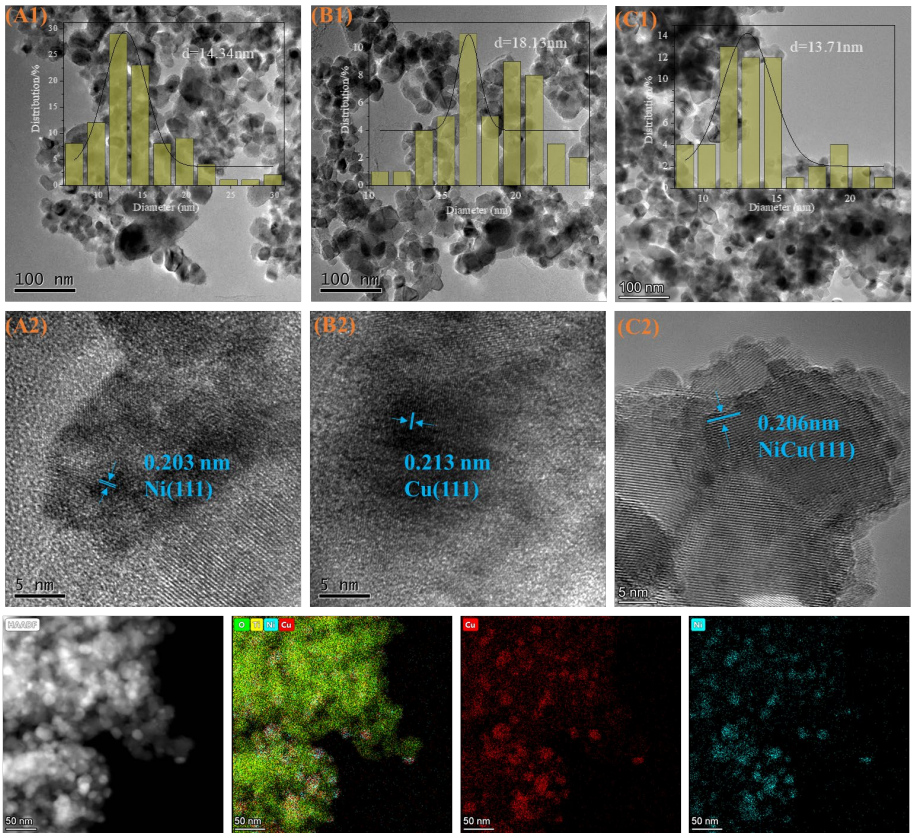

Figure 3. TEM photographs of the catalysts: IM-Ni/TiO_2(A1, A2), IM-Cu/TiO_2(B1, B2) and IM-NiCu/TiO_2(C1, C2). And mapping photographs of the IM-NiCu/TiO_2 catalyst (third row).

An H_2-TPR analysis was carried out on the Ni/TiO_2, Cu/TiO_2 and NiCu/TiO_2 catalysts calcined at 450°C before reduction. As shown in Figure 4 a, the Ni/TiO_2 exhibited two reduction peaks at 369 and 565°C, the former broad reduction peak has corresponded to the reduction of NiO species, which has a stronger interaction with TiO_2 support. And the latter weak shoulder is attributed to the well dispersed NiO species having weak interaction with the TiO_2 support[31, 32]. In the case of the Cu/TiO_2, it is shown that four reduction peaks were observed at 175, 242, 335 and 541°C, the lower temperature reduction peak is attributed to the CuOx species. In contrast, 242 and 335°C are assigned to the high dispersed bulk CuO and large CuO species, respectively[32, 33]. In addition, the highest reduction peak is similar to Ni/TiO_2, which is attributed to the well dispersed CuO species having weak interaction with the TiO_2 support.

Compared with the monometallic Ni/TiO_2 and Cu/TiO_2, the reduction peaks of NiCu/TiO_2 catalyst are shifted to a lower temperature, suggesting that the intimate interaction between Ni and Cu species, the results is consistent with the TEM and the XPS analyses. For the NiCu/TiO_2 catalyst, three reduction peaks can be observed at 157, 242 and 366°C, the sharp reduction peak is attributed to the CuOx species, which is lower than that peak in the Cu/TiO_2. The second peak matches the high dispersed bulk CuO species, which is weakly shifted toward the lower temperature than the Cu/TiO_2 catalyst. And the third reduction peak is assigned to the reduction of NiO species, which significantly shifted to a lower temperature than Ni/TiO_2 catalyst[31, 32]. Interestingly, there have no peaks at the high temperature (541 and 565°C) in the NiCu/TiO_2 catalyst. The intimate interaction of Ni and Cu species must enhance the interaction between the NiCu cluster and TiO_2 support, which the following adsorption energies calculation can also provide.

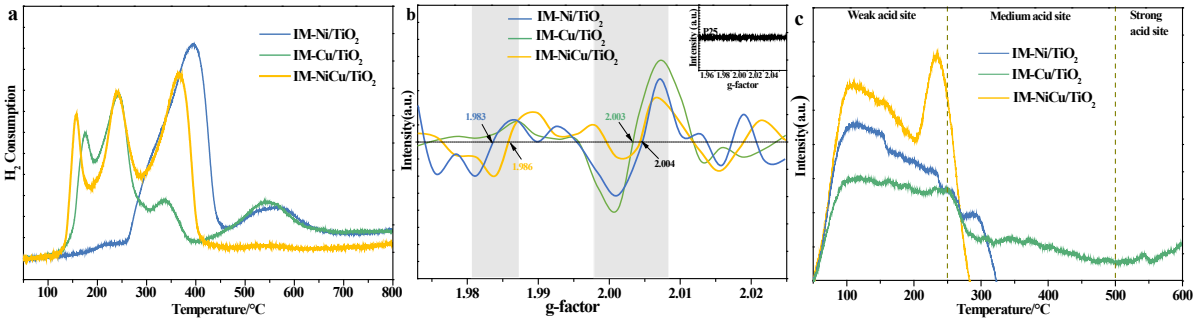

Figure 4. H_2-TPR profiles(a), EPR spectra (b) and NH_3-TPD profiles (c) of the IM-Ni/TiO_2, IM-Cu/TiO_2 and IM-NiCu/TiO_2 catalysts.

EPR spectra were carried out to detect the presence of O_vs, the results are shown in Figure 4 b, the signal of g=1.98-1.99 attributed to the bulk Ti^{3+}, and the signal of g=2.00-2.01 represent the surface O_vs[34]. As the EPR curves show, the support TiO_2 is EPR-silent, the monometallic Ni/TiO_2 catalyst with a relatively weak EPR signal at g=1.983, but the monometallic Cu/TiO_2 without any signal at g=1.983. Compared with Ni/TiO_2 catalyst, the NiCu/TiO_2 catalyst with a weak shifted to g=1.986, indicating that Ni metal can introduce the O_vs into the bulk of TiO_2 during the reduction processes, and

the Cu can be shifted the signal means the interaction between the Ni and Cu metal. Additionally, the monometallic Cu/TiO_2 catalyst shows a strong EPR signal a g=2.003, suggesting the occurrence of surface O_vs species. And both the Ni/TiO_2 and NiCu/TiO_2 catalyst are shown EPR signal at g=2.004 with the intensity Ni/TiO_2 > NiCu/TiO_2. The Cu/TiO_2 catalyst with a strong surface O_vs signal might to the Cu metal migrate O_vs from bulk into the surface. And the NiCu/TiO_2 catalyst with a weaker O_vs signal is a result of the NiCu cluster most likely adsorption on the surface O_vs site, which our DFT calculation can further demonstrate.

The BET analysis of the Ni, Cu and NiCu catalysts are listed in Table 1 and Table S3. The results showed that most of the catalysts with S_{BET} =40.0-60.0 m^2/g, and the NiCu anchored on the R-TiO_2 with a lower S_{BET} =21.9 m^2/g, indicating that the crystal structure mainly dominated hydrogenation reaction. Additionally, NH_3-TPD was also performed to determine the acid strength of the Ni, Cu and NiCu catalysts. As we all know, the acid sites were divided into strong (>500°C), medium (250~500°C), and weak (<250°C) acid sites based on the NH_3 adsorption temperature. As shown in Figure 4c, all three catalysts are mainly composed of weak acid sites and a few medium acid sites. Besides this, the intensity of the three catalysts is as follow: NiCu/TiO_2> Ni/TiO_2> Cu/TiO_2, suggesting that the interaction between the Ni and Cu metal can enhance the weak acid sites of the NiCu catalyst.

Catalytic performance on the hydrogenation of fatty acids

The catalytic performance of the Ni/TiO_2 and NiCu/TiO_2 catalysts are displayed in Figure 5. Under the reaction conditions shown in Figure 5 and Table S4, the Ni/TiO_2 and NiCu/TiO_2 catalysts can hydrogenate fatty acid into C_{17}, C_{18} alkane, and C_{18} alcohol. Firstly, fatty acid can be hydrogenation to C_{18} aldehyde intermediate, then the intermediate can be decarbonylation to produce C_{17} alkane [that is RCOOH→ RCOH→RH], or the intermediate can be hydrogenation into C_{18} alcohol [that is RCOOH→RCOH→RCH_2OH], it also can be further hydrodehydration into C_{18} alkane [that is RCOOH→RCOH→RCH_2OH→RCH_3]. As Figure 5 shows, both Ni/TiO_2 and

$NiCu/TiO_2$ catalysts can select fatty acid hydrogenation into alkane and alcohol. It can convert fatty acid into C_{18} and C_{17} alkanes under a higher reaction temperature, and in contrast, it can produce C_{18} alcohol under a lower reaction temperature (Figures 5 a and b). And the $NiCu/TiO_2$ catalyst showed higher fatty alcohol production activity than the Ni/TiO_2 catalyst. For example, $NiCu/TiO_2$ catalyst showed the C_{18} alcohol yield of 50.8% and 41.0% at 215 and 230°C, higher than that of 38.5% and 12.5% of Ni/TiO_2 catalyst. And it is also should note that the alcohol can be reacted with unconverted acid into easter, thus the alcohol yield is an important index in the alcohol production. The above results indicate that the interaction of Ni and Cu can promote the production of C_{18} alcohol.

The influence of reaction conditions on the production of alcohol by NiCu catalysts was studied with the superior catalyst and the influence of support on the production reaction was firstly investigated, results are listed in Table S 4-6. It reveals that TiO_2 is greatly active in the hydrogenation of fatty acids, probably due to the special structure between TiO_2 and NiCu cluster. After that, the alcohol production conditions were optimized and the results are shown in Figure 5, revealing that the alcohol yield can reach 78.2% at 205°C, 4 MPa and 12 h.

Additionally, the polymorphic phase influence of TiO_2 (A-TiO_2 and R-TiO_2) on alcohol production was also studied. As shown in Figure 5 d-f, both P25 and R-TiO_2 are exhibit greatly catalytic performance toward the production of C18 alcohol. The highest yield of alcohol is 78.2% by using P25, and it can be reached for 66.6% while using R-TiO_2 as support, but which drastically reduced to lower 20% by using A-TiO_2 as support. We can attribute this change in catalytic performance to the R-TiO_2 as support can reverse charge transfer direction between metal and TiO_2 support (it can be supported by following DFT calculation results). Besides this, to be able to the electronic effect on NiCu catalysts. The catalyst preparation method was also investigated. As shown in the Figure 5 h-i, a series of NiCu catalysts were used to convert fatty acid into fatty acid alcohol under 215°C, 6 h and 4 MPa H_2, the results corroborate that catalyst activity of all kinds of NiCu/R-TiO_2 is higher than that

NiCu/A-TiO_2, which emphasizes the importance of rutile phases in the hydrogenation reaction.

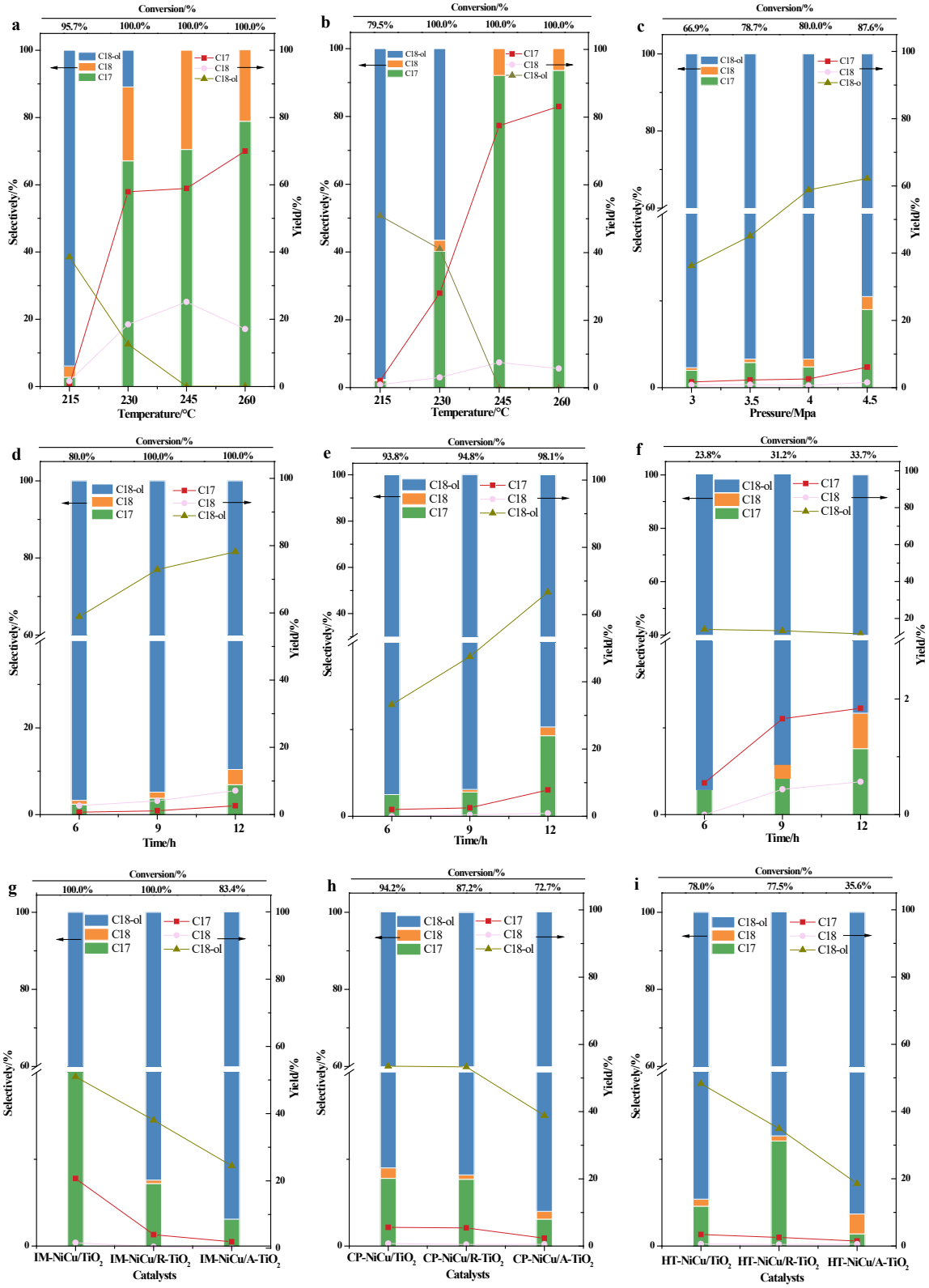

Figure 5. Conversion rate of the fatty acid hydrogenation by different catalysts, selectively and yield of the C_{18}, C_{17} alkane and fatty alcohol for hydrogenation of fatty acid under the condition: (a): Ni/TiO_2, 3 MPa H_2 and 6 h; (b): NiCu/TiO_2, 3 MPa H_2 and 6 h; (c): NiCu/TiO_2, 205°C and 6 h; (d): NiCu/TiO_2, 205°C and 4 MPa H_2; (e): NiCu/A-TiO_2, 205°C and 4 MPa H_2; (f): NiCu/R-TiO_2, 205°C and 4 MPa H_2; (g-i): 215°C, 6 h and 4 MPa H_2. All the results are based on more than three experiments.

Electronic structures investigation

Electronic structure and chemical states were investigated by XPS and DFT calculation. As shown in the XPS spectra in Figure 6 a, the Ti 2P of NiCu catalysts can be decomposed into two pairs of peaks, including Ti^{3+} (~457.9 and ~463.6 eV) and Ti^{4+} (~458.9 and ~464.6 eV), the lower banding energy Ti^{3+} is attributed to the oxygen-deficient phase of TiO_2 with reduced Ti. And the Ti^{3+} peaks of NiCu/R-TiO_2 catalyst were shifted to lower BE than NiCu/A-TiO_2 catalyst, which implies a higher concentration of anionic vacancies on the R-TiO_2 surface. The O1s spectra of the two catalysts in Figure 5 b, lower peaks were attributed to the oxygen vacancies, and the vacancies ratio of the R-TiO_2 is higher than that A-TiO_2, which is consistent with the Ti 2p results. Additionally, the Ni 2p and Cu 2p of the two catalysts are shown in Figure 6 c and d, the Ni^0 $2p_{3/2}$ peaks of NiCu/R-TiO_2 catalyst is almost the same as the NiCu/A-TiO_2 catalyst. Still, the Cu^0 $2p_{3/2}$ of NiCu/R-TiO_2 catalyst can be shifted into lower banding energy than NiCu/A-TiO_2 catalyst, indicating that Cu can promote the electron density change of the NiCu cluster on the R-TiO_2 surface.

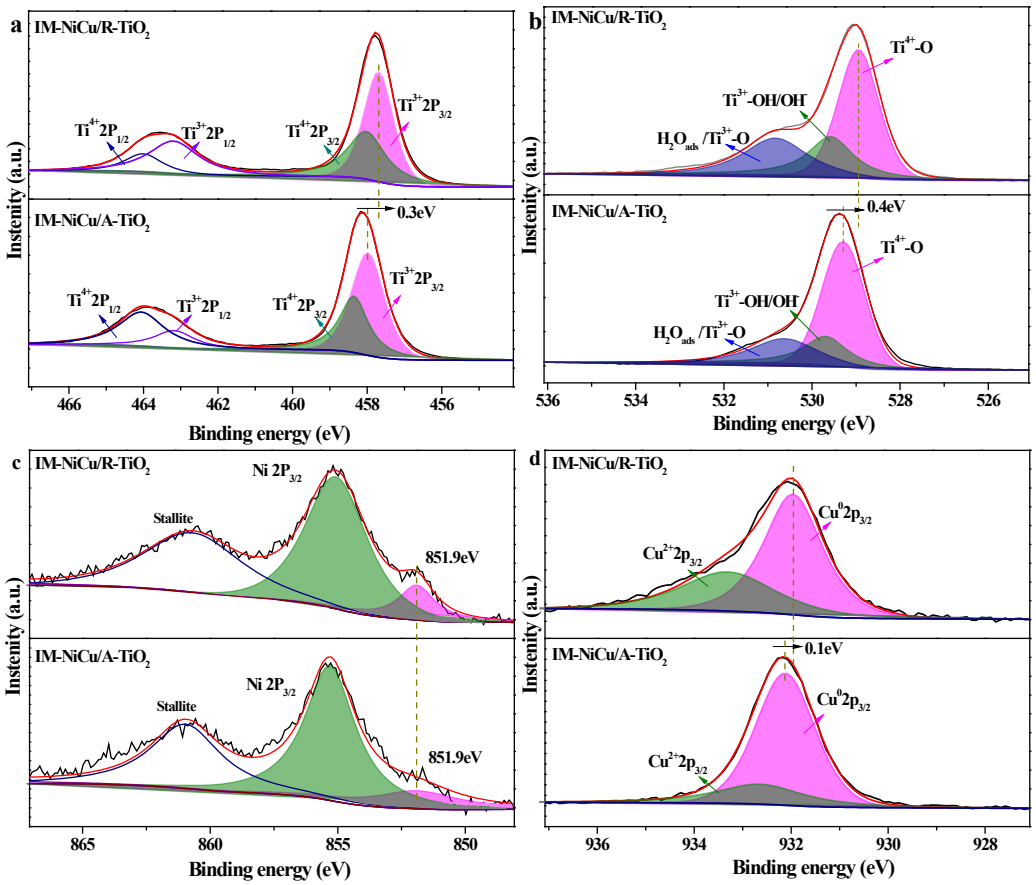

Figure 6. XPS spectra of Ti 2p (a), O 1s (b), Ni 2p (c) and Cu 2p(d) of IM-NiCu/A-TiO_2 and IM-NiCu/R-TiO_2 catalysts.

The electron density of Ni and NiCu clusters on the pristine and oxygen-deficient TiO_2, including R-TiO_2 (rutile)and A-TiO_2 (anatase), were investigated by DFT calculation. Eight model systems of Ni and NiCu support pristine and oxygen-deficient anatase and rutile were studied (Figures 7 and 8). It is found that the stability of NiCu cluster can be significantly enhanced compared with Ni support on TiO_2 surface due to all the adsorption energy of NiCu cluster being higher than that of Ni cluster for 2.6-5.7 eV. Additionally, the electronic property of Ni and NiCu cluster changes on the four kinds of TiO_2. On pristine A-TiO_2 surface, the Ni and NiCu clusters carried positive charges of approximately 0.79 and 1.33 eV, and they can carry 0.45 and 0.58 eV positive charges on pristine R-TiO_2 surface, respectively. It was reported that the electrons could transfer from the metal cluster into support owing to the strong metal-support

interaction[35]. However, Ni and NiCu clusters' charges can be decreased while they are carried by the oxygen-deficient TiO_2. On the oxygen-deficient A-TiO_2 surface, the electrons of Ni and NiCu clusters could reduce to 0.71 and 0.58 eV, respectively. Even the Ni and NiCu clusters could carry a negative charge for 0.30 and 0.22 eV. At the same time, they are supported by oxygen-deficient R-TiO_2, which indicates that electrons initially trapped in the oxygen vacancies partially transfer to the Ni and NiCu clusters. What's more, the electrons reversal between cluster and support was carried out in the oxygen-deficient R-TiO_2 system, leading to the Ni and NiCu clusters becoming negatively charged.

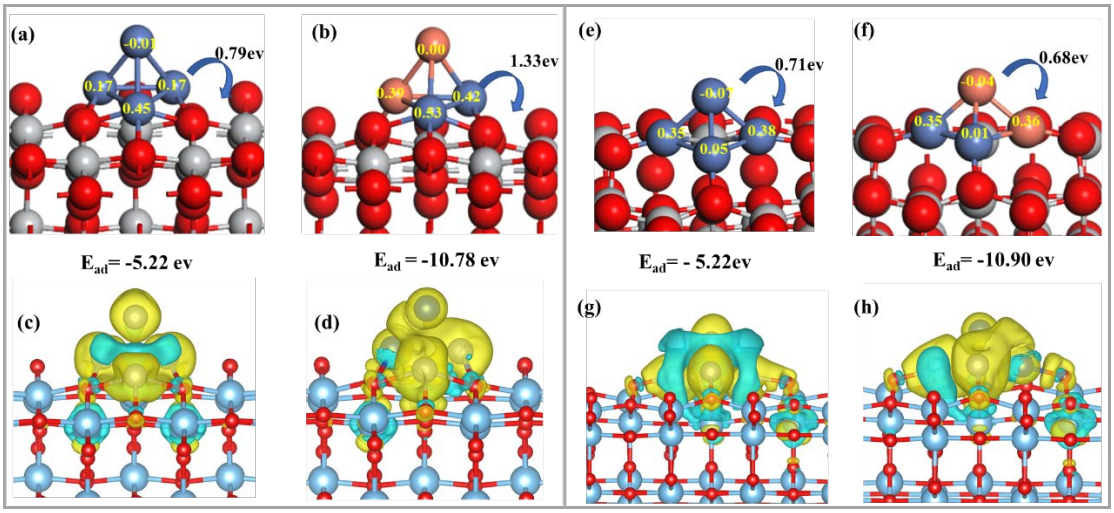

Figure 7. Structure and electron density of a Ni and NiCu cluster supported on anatase surface (a)-(d): (a) Ni clusters connected to pristine anatase via O atom; (b) NiCu clusters connected directly to pristine anatase via O atom; (c) Electron density distribution of (a); (d) Electron density distribution of (b). (e) Ni clusters connected to oxygen-deficient anatase; (b) NiCu clusters connected directly to oxygen-deficient anatase; (g) Electron density distribution of (e); (h) Electron density distribution of (f)Blue, Ni; Red, O; Orange, Cu; gray, Ti;
Turquoise, positive charge; Yellow, negative charge.

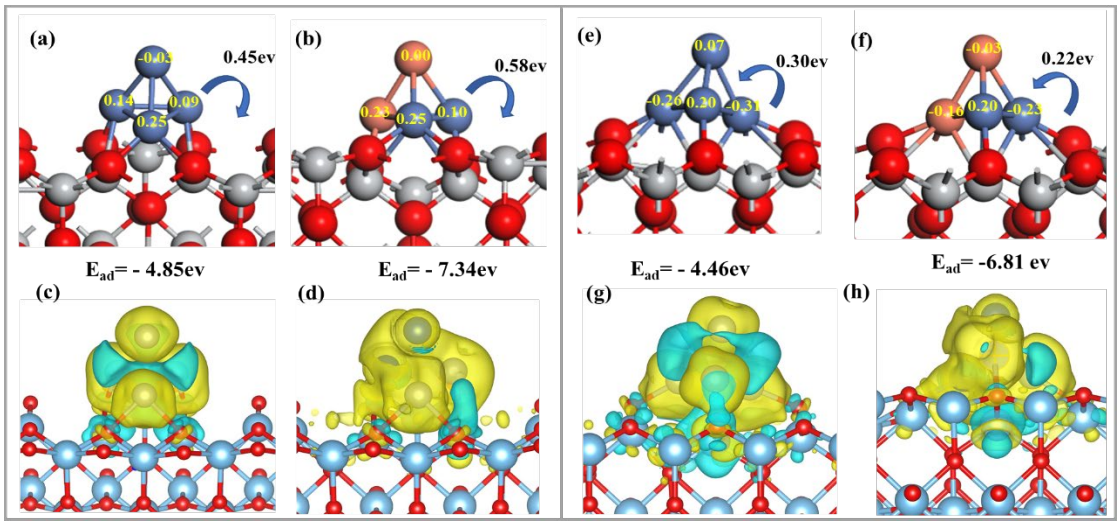

Figure. 8. Structure and electron density of a Ni and NiCu cluster supported on rutile surface (a)-(d): (a) Ni clusters connected to pristine anatase via O atom; (b) NiCu clusters connected directly to pristine rutile via O atom; (c) Electron density distribution of (a); (d) Electron density distribution of (b). (e) Ni clusters connected to oxygen-deficient rutile; (b) NiCu clusters connected directly to oxygen-deficient rutile; (g) Electron density distribution of (e); (h) Electron density distribution of (f)Blue, Ni; Red, O; Orange, Cu; gray, Ti;
Turquoise, positive charge; Yellow, negative charge.

Hydrogenation reaction mechanism

Based on the characterization, tests results, experiment data and DFT calculations, we proposed the NiCu/TiO_2 catalytic reaction mechanism. As shown in Scheme 2, active sites were composite by the metal and oxygen vacancies, the carboxylic acid group of the fatty acid is usually adsorbed on the oxygen vacancy and then undergoes the hydrodeoxygenation reaction to formation of the intermediate-aldehyde (Scheme 2a Path1). After that, the aldehyde conversion into alcohol via hydrogenation (Scheme 2a Path1-2), or alkane via decarbonylation (Scheme 2a Path1-1). In this work, the XPS and DFT calculations demonstrate that part of the NiCu clusters, anchored on rutile surface oxygen vacancies, will carry the negative charge. Thus, the negative NiCu and positive Ti formation of the active site is denoted as M^{-}-O_v-Ti^{+}(M=NiCu cluster), leading NiCu cluster with the higher capability to heterolysis H_2 to produce H^{+}-M^{-}-O_v-

Ti^{+}-H^{-} active species. Therefore, higher alcohol yield can be obtained due to the higher H^{+}-M^{-}-O_v-Ti^{+}-H^{-} active species density. And in contrast, under a higher reaction temperature, the more active NiCu cluster was more in favor of homolysis the H_2 for cleavage of the C-C bond to produce alkane products.

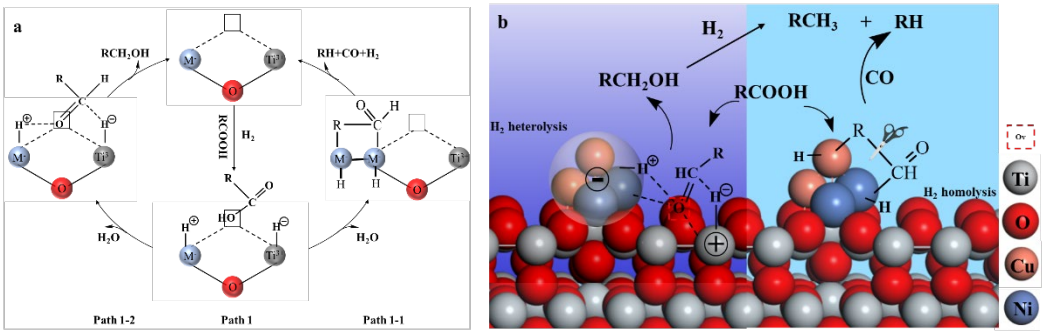

Scheme 2. Proposed mechanism of hydrogenation of fatty acids on the NiCu/R-TiO_2 catalysts.

Conclusions

Herein, Ni/TiO_2 and a series of NiCu/TiO_2 catalysts were prepared by impregnation, hydrothermal, and coprecipitation methods for selective hydrogenation of fatty acids into diesel-like alkane and high-valuable fatty alcohol. The catalysts' structural characteristics and electronic properties are systematically studied by XRD, TEM and Mapping, XPS, H_2-TPR, EPR, BET, NH_3-TPD and DFT calculation. Experimental results indicated that NiCu/TiO_2 (P25) prepared by impregnation possessed superior catalytic activities with a higher fatty alcohol yield of 78.2% and alkane yield of 85.0%, respectively. The conversion yield variation relates to the crystal type, oxygen deficiency of the TiO_2 and the interaction between Ni and Cu, finally affecting the electron density of metal clusters and structure. Bader analyses demonstrate that rutile with oxygen vacancies can transfer charge reversal between Ni/NiCu cluster and rutile support. The metal clusters anchored on oxygen-vacancies-rutile surface endowing negative charges can promote fatty alcohol production. And the more active NiCu cluster will work for alkane production under a higher reaction temperature. Thus, the normal NiCu clusters anchored on TiO_2 surface (especially rutile phase) can improve their temperature-sensitive activity for a higher alkane or alcohol

yield. Our work provides a new strategy for designing highly efficient catalysts to convert the bio-derived fatty acid into fatty alcohol or alkane.

ASSOCIATED CONTENT

Supporting Information: Catalysts preparation section. XRD patterns of some reduced catalysts (Figure S1), The data of the actual loading of all Ni or Cu on the TiO_2 support (Table S1). The ratio of O1S species in Ni, Cu and NiCu catalysts calculated from XPS spectra (Table S2), and BET analysis of the NiCu catalysts (Table S3). The conversion rate of the fatty acid, selectively and yield of the C_{18}, C_{17} alkane and fatty alcohol for hydrogenation of fatty acid over different catalysts or under different conditions (Table S4-6).

AUTHOR INFORMATION

Corresponding Author

Junming Xu - Institute of Chemical Industry of Forest Products, Chinese Academy of Forestry; Key Lab. of Biomass Energy and Material, Jiangsu Province; Key Lab. of Chemical Engineering of Forest Products, National Forestry and Grassland Administration; National Engineering Lab. for Biomass Chemical Utilization, Nanjing 210042, China. Co-Innovation Center of Efficient Processing and Utilization of Forest Resources, Nanjing Forestry University, Nanjing 210037, China. Email: xujunming@icifp.cn.

Authors

Feng Long - Institute of Chemical Industry of Forest Products, Chinese Academy of Forestry; Key Lab. of Biomass Energy and Material, Jiangsu Province; Key Lab. of Chemical Engineering of Forest Products, National Forestry and Grassland Administration; National Engineering Lab. for Biomass Chemical Utilization, Nanjing 210042, China.

Xincheng Cao- Institute of Chemical Industry of Forest Products, Chinese Academy

of Forestry; Key Lab. of Biomass Energy and Material, Jiangsu Province; Key Lab. of Chemical Engineering of Forest Products, National Forestry and Grassland Administration; National Engineering Lab. for Biomass Chemical Utilization, Nanjing 210042, China.

Xia Jiang- Institute of Chemical Industry of Forest Products, Chinese Academy of Forestry; Key Lab. of Biomass Energy and Material, Jiangsu Province; Key Lab. of Chemical Engineering of Forest Products, National Forestry and Grassland Administration; National Engineering Lab. for Biomass Chemical Utilization, Nanjing 210042, China.

Peng Liu- Institute of Chemical Industry of Forest Products, Chinese Academy of Forestry; Key Lab. of Biomass Energy and Material, Jiangsu Province; Key Lab. of Chemical Engineering of Forest Products, National Forestry and Grassland Administration; National Engineering Lab. for Biomass Chemical Utilization, Nanjing 210042, China.

Jianchun Jiang - Institute of Chemical Industry of Forest Products, Chinese Academy of Forestry; Key Lab. of Biomass Energy and Material, Jiangsu Province; Key Lab. of Chemical Engineering of Forest Products, National Forestry and Grassland Administration; National Engineering Lab. for Biomass Chemical Utilization, Nanjing 210042, China. Co-Innovation Center of Efficient Processing and Utilization of Forest Resources, Nanjing Forestry University, Nanjing 210037, China.

Xiaolei Zhang - Department of Chemical and Process Engineering, University of Strathclyde, Glasgow, G11XJ, UKs

Notes

The authors declare no competing financial interest.

ACKNOWLEDGMENTS

Our works were supported by the "National Key Research and Development Project" (Grant No. 2019YFB1504005)

References

(1) Jun Ni; Wenhua Leng; Jun Mao; Jianguo Wang; Jianyi Lin; Jiang, D. Tuning electron density of metal nickel by support defects in Ni/ZrO_2 for selective hydrogenation of fatty acids to alkanes and alcohols. *Applied Catalysis B: Environmental* **2019**, *253*, 170-178. DOI: 10.1016/j.apcatb.2019.04.043.

(2) Pritchard, J.; Filonenko, G. A.; van Putten, R.; Hensen, E. J.; Pidko, E. A. Heterogeneous and homogeneous catalysis for the hydrogenation of carboxylic acid derivatives: history, advances and future directions. *Chemical Society Reviews* **2015**, *44* (11), 3808-3833. DOI: 10.1039/c5cs00038f.

(3) Zhipeng Huang; Zhitong Zhao; Chaofeng Zhang; Jianmin Lu; Huifang Liu; Nengchao Luo; Jian Zhang; Wang, F. Enhanced photocatalytic alkane production from fatty acid decarboxylation via inhibition of radical oligomerization. *Nature Catalysis* **2020**, *3* (2), 170-178. DOI: 10.1038/s41929-020-0423-3. Long, F.; Liu, W.; Jiang, X.; Zhai, Q.; Cao, X.; Jiang, J.; Xu, J. State-of-the-art technologies for biofuel production from triglycerides: A review. *Renewable and Sustainable Energy Reviews* **2021**, *148*, 111269. DOI: 10.1016/j.rser.2021.111269. Long, F.; Zhai, Q.; Liu, P.; Cao, X.; Jiang, X.; Wang, F.; Wei, L.; Liu, C.; Jiang, J.; Xu, J. Catalytic conversion of triglycerides by metal-based catalysts and subsequent modification of molecular structure by ZSM-5 and Raney Ni for the production of high-value biofuel. *Renewable Energy* **2020**, *157*, 1072-1080. DOI: 10.1016/j.renene.2020.05.117.

(4) Coumans, A. E.; Hensen, E. J. M. A model compound (methyl oleate, oleic acid, triolein) study of triglycerides hydrodeoxygenation over alumina-supported NiMo sulfide. *Applied Catalysis B: Environmental* **2017**, *201*, 290-301. DOI: https://doi.org/10.1016/j.apcatb.2016.08.036.

(5) Wang, F.; Jiang, J.; Wang, K.; Zhai, Q.; Long, F.; Liu, P.; Feng, J.; Xia, H.; Ye, J.; Li, J.; et al. Hydrotreatment of lipid model for diesel-like alkane using nitrogen-doped mesoporous carbon-supported molybdenum carbide. *Applied Catalysis B: Environmental* **2019**, *242*, 150-160. DOI: 10.1016/j.apcatb.2018.09.077. Jeong, H.; Shin, M.; Jeong, B.; Jang, J. H.; Han, G. B.; Suh, Y.-W. Comparison of activity and stability of supported Ni2P and Pt catalysts in the hydroprocessing of palm oil into normal paraffins. *Journal of Industrial and Engineering Chemistry* **2020**, *83*, 189-199. DOI: https://doi.org/10.1016/j.jiec.2019.11.027. Phimsen, S.; Kiatkittipong, W.; Yamada, H.; Tagawa, T.; Kiatkittipong, K.; Laosiripojana, N.; Assabumrungrat, S. Nickel sulfide, nickel phosphide and nickel carbide catalysts for bio-hydrotreated fuel production. *Energy Conversion and Management* **2017**, *151*, 324-333. DOI: https://doi.org/10.1016/j.enconman.2017.08.089.

(6) Ameen, M.; Azizan, M. T.; Yusup, S.; Ramli, A.; Yasir, M. Catalytic hydrodeoxygenation of triglycerides: An approach to clean diesel fuel production. *Renewable and Sustainable Energy Reviews* **2017**, *80*, 1072-1088. DOI: 10.1016/j.rser.2017.05.268. Rakmae, S.; Osakoo, N.; Pimsuta, M.; Deekamwong, K.; Keawkumay, C.; Butburee, T.; Faungnawakij, K.; Geantet, C.; Prayoonpokarach, S.; Wittayakun, J.; et al. Defining nickel phosphides supported on sodium mordenite for hydrodeoxygenation of palm oil. *Fuel Processing Technology* **2020**, *198*, 106236. DOI: https://doi.org/10.1016/j.fuproc.2019.106236.

(7) Han, D.; Yin, W.; Wang, S.; Xia, S. Fabrication of a NiFe Alloy Oxide Catalyst via Surface Reconstruction for Selective Hydrodeoxygenation of Fatty Acid to Fatty Alcohol. *ACS Sustainable Chemistry & Engineering* **2021**, *9* (44), 15027-15041. DOI: 10.1021/acssuschemeng.1c05919.

(8) Papageridis, K. N.; Charisiou, N. D.; Douvartzides, S.; Sebastian, V.; Hinder, S. J.; Baker, M. A.;

AlKhoori, S.; Polychronopoulou, K.; Goula, M. A. Promoting effect of CaO-MgO mixed oxide on Ni/γ-Al2O3 catalyst for selective catalytic deoxygenation of palm oil. *Renewable Energy* **2020**, *162*, 1793-1810. DOI: https://doi.org/10.1016/j.renene.2020.09.133. Papageridis, K. N.; Charisiou, N. D.; Douvartzides, S. L.; Sebastian, V.; Hinder, S. J.; Baker, M. A.; AlKhoori, S.; Polychronopoulou, K.; Goula, M. A. Effect of operating parameters on the selective catalytic deoxygenation of palm oil to produce renewable diesel over Ni supported on Al2O3, ZrO2 and SiO2 catalysts. *Fuel Processing Technology* **2020**, *209*, 106547. DOI: https://doi.org/10.1016/j.fuproc.2020.106547.

(9) Voeste, T.; Buchold, H. Production of fatty alcohols from fatty acids. *Journal of the American Oil Chemists' Society* **1984**, *61* (2), 350-352. DOI: https://doi.org/10.1007/BF02678794. Xiao, Y.; Liu, Y.; Zhang, X.; Hou, J.; Liu, X.; Yuan, Y.; Liao, X. Highly effective CoOx for catalytic transfer hydrogenation of plant oil to fatty alcohols. *Catalysis Communications* **2022**, *165*, 106448. DOI: https://doi.org/10.1016/j.catcom.2022.106448.

(10) Kandel, K.; Chaudhary, U.; Nelson, N. C.; Slowing, I. I. Synergistic Interaction between Oxides of Copper and Iron for Production of Fatty Alcohols from Fatty Acids. *ACS Catalysis* **2015**, *5* (11), 6719-6723. DOI: 10.1021/acscatal.5b01664.

(11) Zhang, Z.; Zhou, F.; Chen, K.; Fu, J.; Lu, X.; Ouyang, P. Catalytic In Situ Hydrogenation of Fatty Acids into Fatty Alcohols over Cu-Based Catalysts with Methanol in Hydrothermal Media. *Energy & Fuels* **2017**, *31* (11), 12624-12632. DOI: 10.1021/acs.energyfuels.7b01621.

(12) Fonseca Benítez, C. A.; Mazzieri, V. A.; Sánchez, M. A.; Benitez, V. M.; Pieck, C. L. Selective hydrogenation of oleic acid to fatty alcohols on Rh-Sn-B/Al_2O_3 catalysts. Influence of Sn content. *Applied Catalysis A: General* **2019**, *584*. DOI: 10.1016/j.apcata.2019.117149.

(13) Rodina, V. O.; Ermakov, D. Y.; Saraev, A. A.; Reshetnikov, S. I.; Yakovlev, V. A. Influence of reaction conditions and kinetic analysis of the selective hydrogenation of oleic acid toward fatty alcohols on Ru-Sn-B/Al 2 O 3 in the flow reactor. *Applied Catalysis B: Environmental* **2017**, *209*, 611-620. DOI: 10.1016/j.apcatb.2017.03.012. Luo, Z.; Bing, Q.; Kong, J.; Liu, J.-y.; Zhao, C. Mechanism of supported Ru_3Sn_7 nanocluster-catalyzed selective hydrogenation of coconut oil to fatty alcohols. *Catalysis Science & Technology* **2018**, *8* (5), 1322-1332. DOI: 10.1039/c8cy00037a.

(14) Martínez-Prieto, L. M.; Puche, M.; Cerezo-Navarrete, C.; Chaudret, B. Uniform Ru nanoparticles on N-doped graphene for selective hydrogenation of fatty acids to alcohols. *Journal of Catalysis* **2019**, *377*, 429-437. DOI: 10.1016/j.jcat.2019.07.040.

(15) Rozmysłowicz, B.; Kirilin, A.; Aho, A.; Manyar, H.; Hardacre, C.; Wärnå, J.; Salmi, T.; Murzin, D. Y. Selective hydrogenation of fatty acids to alcohols over highly dispersed ReO_x/TiO_2 catalyst. *Journal of Catalysis* **2015**, *328* 197–207. DOI: 10.1016/j.jcat.2015.01.003.

(16) Manyar, H. G.; Paun, C.; Pilus, R.; Rooney, D. W.; Thompson, J. M.; Hardacre, C. Highly selective and efficient hydrogenation of carboxylic acids to alcohols using titania supported Pt catalysts. *Chemical communications* **2010**, *46* (34), 6279-6281. DOI: https://doi.org/10.1039/C0CC01365J.

(17) Ullrich, J.; Breit, B. Selective hydrogenation of carboxylic acids to alcohols or alkanes employing a heterogeneous catalyst. *ACS Catalysis* **2018**, *8* (2), 785-789. DOI: 10.1021/acscatal.7b03484.

(18) Wang, L.; Niu, X.; Chen, J. SiO_2 supported Ni-In intermetallic compounds: Efficient for selective hydrogenation of fatty acid methyl esters to fatty alcohols. *Applied Catalysis B: Environmental* **2020**, *278*. DOI: 10.1016/j.apcatb.2020.119293.

(19) Onyestyák, G.; Harnos, S.; Kalló, D. Indium, as an efficient co-catalyst of Cu/Al_2O_3 in the selective hydrogenation of biomass derived fatty acids to alcohols. *Catalysis Communications* **2012**, *26*, 19-24. DOI: 10.1016/j.catcom.2012.04.023.

(20) Cao, X.; Long, F.; Zhang, G.; Xu, J.; Jiang, J. Selective Hydrogenation of Methyl Palmitate to Cetyl Alcohol via Ternary Synergistic Catalysis of Ni, Oxygen Vacancies, and Lewis Acid Sites under Mild Reaction Conditions. *ACS Sustainable Chemistry & Engineering* **2021**, *9* (29), 9789-9801. DOI: 10.1021/acssuschemeng.1c02181. Cao, X.; Long, F.; Zhai, Q.; Zhao, J.; Xu, J.; Jiang, J. Heterogeneous Ni and MoOx co-loaded CeO_2 catalyst for the hydrogenation of fatty acids to fatty alcohols under mild reaction conditions. *Fuel* **2021**, *298*. DOI: 10.1016/j.fuel.2021.120829.

(21) Cao, X.; Long, F.; Wang, F.; Zhao, J.; Xu, J.; Jiang, J. Chemoselective decarboxylation of higher aliphatic esters to diesel-range alkanes over the $NiCu/Al_2O_3$ bifunctional catalyst under mild reaction conditions. *Renewable Energy* **2021**, *180*, 1-13. DOI: 10.1016/j.renene.2021.08.004.

(22) Li, W.; Ye, L.; Long, P.; Chen, J.; Ariga, H.; Asakura, K.; Yuan, Y. Efficient Ru–Fe catalyzed selective hydrogenolysis of carboxylic acids to alcoholic chemicals. *RSC advances* **2014**, *4* (55), 29072-29082. DOI: 10.1039/c4ra03201b.

(23) A, G. K.; b, J. F. Efficiency of ab-initio total energy calculations for metals and semiconductors using a plane-wave basis set. *Computational Materials Science* **1996**, *6* (1), 15-50. DOI: 10.1016/0927-0256(96)00008-0. Kresse, G. G.; Furthmüller, J. J. Efficient Iterative schemes for Ab Initio total-energy calculations using a plane-wave basis set. *Physical review. B* **1996**, *54*, 11169. DOI: 10.1103/physrevb.54.11169. Perdew, J. P.; Wang, Y. Accurate and simple analytic representation of the electron-gas correlation energy. *Physical review B* **1992**, *45* (23), 13244. DOI: 10.1103/physrevb.45.13244.

(24) Blochl, P. E. Projector augmented-wave method. *Physical Review B* **1994**, *50*, 17953-17979. DOI: 10.1103/physrevb.50.17953. Perdew, J. P.; Burke, K.; Ernzerhof, M. Generalized gradient approximation made simple. *Physical Review Letters* **1998**, *77* (18), 3865-3868. DOI: 10.1103/physrevlett.77.3865.

(25) Li, H.; Ren, F.; Liu, J.; Wang, Q.; Li, Q.; Yang, J.; Wang, Y. Endowing single-electron-trapped oxygen vacancy self-modified titanium dioxide with visible-light photocatalytic activity by grafting Fe(III) nanocluster. *Applied Catalysis B Environmental* **2015**, *172*, 37-45. Hao, Y.-n.; Chen, T.; Zhang, X.; Zhou, H.; Ma, Y. Ti-Ti σ bond at oxygen vacancy inducing the deep defect level in anatase TiO_2 (101) surface. *The Journal of Chemical Physics* **2019**, *150* (22), 224702. DOI: 10.1063/1.5108595.

(26) Yang, W.; Yang, X.; Jia, J.; Hou, C.; Gao, H.; Mao, Y.; Wang, C.; Lin, J.; Luo, X. Oxygen vacancies confined in ultrathin nickel oxide nanosheets for enhanced electrocatalytic methanol oxidation. *Applied Catalysis B: Environmental* **2019**, *244*, 1096-1102. DOI: 10.1016/j.apcatb.2018.12.038. Cao, X.; Long, F.; Zhai, Q.; Liu, P.; Xu, J.; Jiang, J. Enhancement of fatty acids hydrodeoxygenation selectivity to diesel-range alkanes over the supported Ni-MoOx catalyst and elucidation of the active phase. *Renewable Energy* **2020**, *162*, 2113-2125. DOI: 10.1016/j.renene.2020.10.052.

(27) Sanjines, R.; Tang, H.; Berger, H.; Gozzo, F.; Margaritondo, G.; Levy, F. Electronic structure of anatase TiO_2 oxide. *Journal of Applied Physics* **1994**, *75* (6), 2945-2951. DOI: https://doi.org/10.1063/1.356190.

(28) Qiu, H.; Ma, X.; Sun, C.; Zhao, B.; Chen, F. Surface oxygen vacancies enriched Pt/TiO_2 synthesized with a defect migration strategy for superior photocatalytic activity. *Applied Surface Science* **2020**, *506*. DOI: 10.1016/j.apsusc.2019.145021.

(29) Takata, Y.; Hidaka, S.; Masuda, M.; Ito, T. Pool boiling on a superhydrophilic surface. *International Journal of Energy Research* **2003**, *27* (2), 111-119. DOI: 10.1002/er.861.

(30) Shen, Y.; Li, L.; Xiao, K.; Xi, J. Constructing three-dimensional hierarchical architectures by integrating carbon nanofibers into graphite felts for water purification. *ACS Sustainable Chemistry*

& Engineering **2016**, *4* (4), 2351-2358. DOI: 10.1021/acssuschemeng.6b00030.

(31) Riaz, N.; Chong, F. K.; Dutta, B. K.; Man, Z. B.; Khan, M. S.; Nurlaela, E. Photodegradation of Orange II under visible light using Cu–Ni/TiO_2: Effect of calcination temperature. *Chemical Engineering Journal* **2012**, *185-186*, 108-119. DOI: 10.1016/j.cej.2012.01.052.

(32) Seemala, B.; Cai, C. M.; Wyman, C. E.; Christopher, P. Support Induced Control of Surface Composition in Cu–Ni/TiO_2 Catalysts Enables High Yield Co-Conversion of HMF and Furfural to Methylated Furans. *ACS Catalysis* **2017**, *7* (6), 4070-4082. DOI: 10.1021/acscatal.7b01095.

(33) Wang, Z.; Brouri, D.; Casale, S.; Delannoy, L.; Louis, C. Exploration of the preparation of Cu/TiO_2 catalysts by deposition–precipitation with urea for selective hydrogenation of unsaturated hydrocarbons. *Journal of Catalysis* **2016**, *340*, 95-106. DOI: 10.1016/j.jcat.2016.05.011.

(34) Qiu, H.; Ma, X.; Sun, C.; Zhao, B.; Chen, F. Surface oxygen vacancies enriched Pt/TiO_2 synthesized with a defect migration strategy for superior photocatalytic activity. *Applied Surface Science* **2020**, *506*, 145021. DOI: 10.1016/j.apsusc.2019.145021. Li, H.; Ren, F.; Liu, J.; Wang, Q.; Li, Q.; Yang, J.; Wang, Y. Endowing single-electron-trapped oxygen vacancy self-modified titanium dioxide with visible-light photocatalytic activity by grafting Fe(III) nanocluster. *Applied Catalysis B: Environmental* **2015**, *172-173*, 37-45. DOI: 10.1016/j.apcatb.2015.02.008.

(35) Wang, B.; Xiong, Y.; Han, Y.; Hong, J.; Zhang, Y.; Li, J.; Jing, F.; Chu, W. Preparation of stable and highly active Ni/CeO_2 catalysts by glow discharge plasma technique for glycerol steam reforming. *Applied Catalysis B: Environmental* **2019**, *249*, 257-265. DOI: https://doi.org/10.1016/j.apcatb.2019.02.074.